HiSST: 3rd International Conference on High-Speed Vehicle Science Technology
14 -19 April 2024, Busan, Korea

Tailored directional porosity in Ceramic Matrix Composites (CMC) for hypersonic applications

F. Kessel[1], Dr. M. Friess[1], C. Rauh[1], Dr. A. Wagner[2]*

[1]German Aerospace Center (DLR), Institute of Structures and Design, Pfaffenwaldring 38-40, 70569 Stuttgart, Germany
[2]German Aerospace Center (DLR), Institute of Aerodynamics and Flow Technology, Bunsenstrasse 10, 37073 Göttingen, Germany
**corresponding author*

Abstract

In the field of hypersonic systems and their missions, the occurring flows impose extreme mechanical and thermal loads on the materials used. At German Aerospace Center (DLR), extensive research is conducted in this area, ranging from design and specification to suitable material developments, and concluding with the proof of concept under realistic conditions in wind tunnels. In recent years, ceramic matrix composites (CMCs) have been investigated for specific aspects of hypersonics. These materials exhibit consistent mechanical behaviour over a wide temperature range (up to 1600 °C), coupled with high damage tolerance and thermal shock resistance, distinguishing them from metals and superalloys. Particularly, special porous C/C-SiC ceramics (carbon-fibre-reinforced carbon with silicon carbide) enable innovative material applications for components in transpiration cooling, fuel injection, or boundary layer transition control. The work presented focuses on the next generation of porous C/C-SiC ceramics currently in development. By deliberately modifying the textile preform, the resulting microstructure and pore morphology are influenced, allowing for control over both the total volume and the orientation of the pores. Relevant parameters influencing porosity have been determined based on the results, and an initial characterization has been conducted. It has been demonstrated that there is a preferred direction of porosity within the sample thickness (Z-axis), and in terms of hypersonic-relevant properties, a supersonic absorption of 0.58 for a frequency of 500 kHz (static pressure of 15 kPa), as well as a length specific flow resistance of 3.4 MPa s/m² and an overall porosity of 12.25 % were determined. Building upon these promising initial findings, the goal is to further expand the understanding of the parameters influencing porosity and to generate a tailored material for different application scenarios by correlating them with hypersonic properties.

Keywords: *Ceramic Matrix Composite, C/C-SiC, OCTRA, Liquid Silicon Infiltration, transpiration cooling, hypersonic boundary layer transition control*

Nomenclature

C – carbon
C/C – carbon fibre reinforced carbon
C/C-SiC – carbon fibre reinforced carbon with silicon carbide
CMC – ceramic matrix composites
CT – computed tomography
LFA – laser flash analysis
RTM – resin transfer moulding
LSI – liquid silicon infiltration
OCTRA – optimized ceramic for hypersonic applications with transpiration cooling
st – stitches
T – temperature
tex – unit for yarns (g/1000m)
TFP – Tailored Fibre Placement

1. Introduction

Hypersonic flows and their extreme mechanical and thermal loads represent some of the most demanding environmental conditions in high-speed systems. Materials suitable for such systems are therefore held to the highest standards, resulting in only a very limited number of materials being considered. One interesting group of materials in this regard are ceramic matrix composites (CMC), which distinguish themselves from metals and superalloys by exhibiting consistent mechanical behaviour over a wide temperature range, coupled with high damage tolerance and thermal shock resistance [1, 2]. Within this group C/C ceramics (carbon fibre reinforced carbon) and porous C/C-SiC ceramics (carbon fibre reinforced carbon with silicon carbide), which have gained particular attention in recent years, offer innovative potential in the realms of transpiration cooling, fuel injection, and hypersonic boundary layer transition [3-7]. The material referred to as OCTRA (Optimized Ceramic for Hypersonic applications with transpiration cooling), as introduced by Dittert et al., falls under this category and has been comprehensively characterized with respect to its hypersonic properties [8]. A crucial criterion for the functionality of the material lies in the porosity and its orientation relative to the flow direction. Traditionally, OCTRA material has been fabricated as a solid block, from which components or samples with desired porosity orientation were machined. While this method allows for tailoring the pore network to suit hypersonic applications, it is associated with costly material production and significant material loss due to machining. The work presented, thus pursues the approach of introducing porosity perpendicular to the ply stack of the material at an early preforming stage of material production. The objective is to identify suitable parameter for influencing material properties through preforming, which is relatively cost-effective compared to adjustments made during subsequent ceramic processing. The approach aims to enhance porosity functionality for the intended application and facilitate the near-net-shape production of potential OCTRA components, and to ultimately minimize their production costs. Initial results from investigations into the preform and the resulting properties are presented in this work.

2. Design of Experiments / Methods

OCTRA is manufactured using the Liquid Silicon Infiltration process (LSI), which comprises three main steps: shaping, pyrolysis, and siliconization [1]. The scheme of the manufacturing process is visualized in **Fig. 1**. In addition to carbon fibre fabrics, hybrid fabrics (combining aramid and carbon roving) are also used. These materials are assembled into layer stacks and then infiltrated and consolidated with a polymer matrix. Following shaping, the pyrolysis stage takes place, during which volatile components are split off at high temperatures (T<900 °C). This primarily affects the matrix (resulting in a remaining C-matrix of approximately 50-60 %) and the aramid fibre (with a carbon residue of approximately 30-50 %). This process results in the creation of a complex pore network, particularly prominent in the former aramid fibre areas. In the subsequent siliconization step, silicon granules are melted (T>1420 °C) and infiltrate the material's pore network through capillary forces. In the contact area between melt and carbon, the reaction to the ceramic SiC matrix takes place [9]. The process concludes with a final high-temperature step, during which any unreacted silicon is removed from the material, thus exposing the pore structure once again.

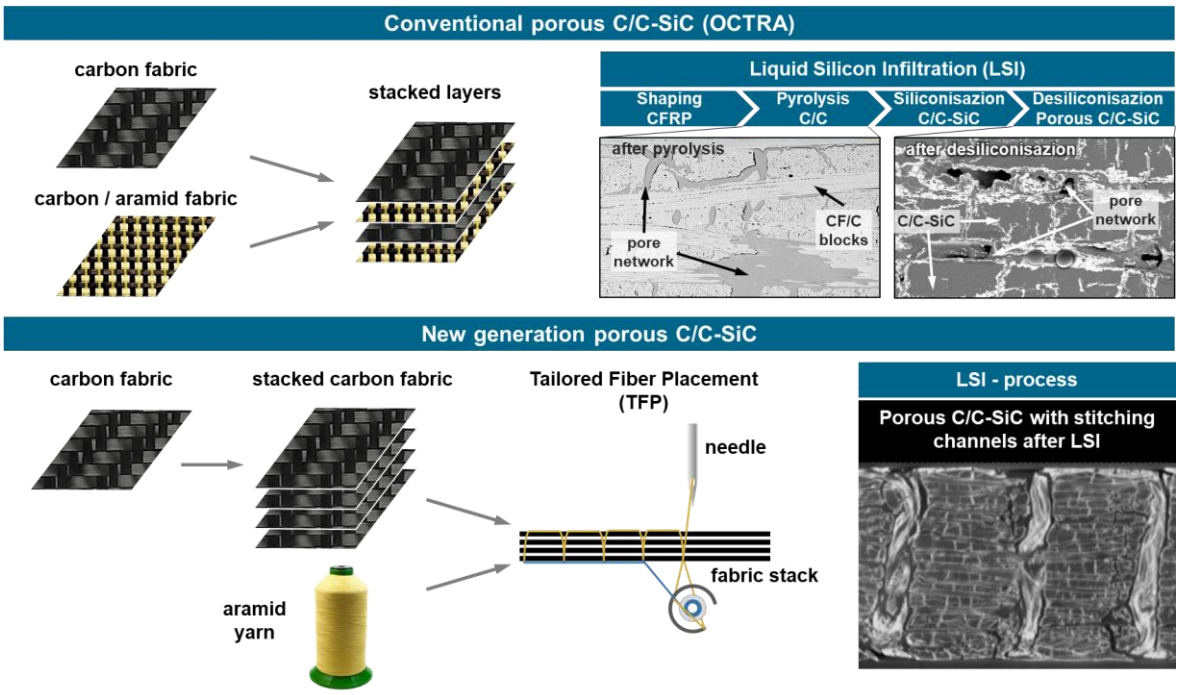

Fig 1. Scheme of the manufacturing process of OCTRA using the LSI process (upper part) and scheme of the new material generation with adapted preform produced via the TFP process (lower part)

The new generation OCTRA utilizes carbon fibre fabric exclusively, eliminating the need for hybrid layers, and achieving adjustable porosity. Aramid fibres are incorporated into the ply stacks through an additional textile process. Two techniques are being investigated for this: tufting and tailored fibre placement (TFP). In both methods, an aramid thread or yarn is stitched through the ply stack, remaining in the area of the piercing channel. According to Dittert et al., porosity forms in the area of the aramid, resulting in a preferential direction perpendicular to the ply stack [8, 10].

For the experimental series, a sample was first produced for each method (tufting and TFP). The resulting porosity in the area of the aramid yarn was determined using micro computed tomography. Anticipating those first results, the TFP manufacturing method was selected, and two parameters were varied: yarn thickness and stitch density. Three yarn thicknesses were chosen: fine (7 tex), medium (36 tex), and coarse (55 tex). Originally, a variation of stitch densities of 25 stitches/cm², 36 stitches/cm², and 50 stitches/cm² was planned. However, to better delineate extreme ranges, the highest stitch density for the medium yarn thickness was omitted, and instead, a lower stitch density of 16 stitches/cm² was added for the coarse yarn. Additionally, to better assess the influence of stitch insertion, a reference sample was also produced, which has no insertions and thus consists solely of carbon layers, unlike regular C/C-SiC but was desiliconized analogously to the other samples. In total, twelve ceramic samples were thus manufactured.

For sample characterization the porosity and density were measured by following Archimedes method (DIN EN 993– 1:1995– 04). The finished materials were further subjected to mechanical testing using the 3-point-bending method according to DIN EN 658-3, to determine the material strength. On selected samples the microstructure was investigated with micro computed tomography with a Phoenix|x-ray nanotom from Waygate Technologies. Additionally, the specific heat capacity and thermal conductivity were determined for the coarse yarn sample with a stich density of 50 st/cm² using the laser flash method according to DIN EN 1159-2. For the same sample, supersonic absorption was analysed following the by Wagner et al. described method [4], as well as the length specific flow resistance was measured with a setup described by Dittert et al. following DIN EN ISO 9053-1 [10].

3. Results

3.1. Comparison between Tufting vs. TFP

The Tufting and TFP samples were manufactured following the production route depicted in **Fig. 1**. To assess the formation of channel structures perpendicular to the ply stack, the samples were compared using µCt. A cross-sectional view of the samples is presented in **Fig. 2**. The tufted sample exhibits needle channels that are diagonal and undulating. Conversely, the TFP sample displays nearly vertical needle channels, devoid of undulations. The most prominent feature in both samples is the needle channel, with additional interlaminar porosity observed horizontally. Both samples exhibit a C/C block structure, typically for C/C-SiC material, which is necessary for achieving the fracture-tough behaviour of fibre-reinforced ceramics.

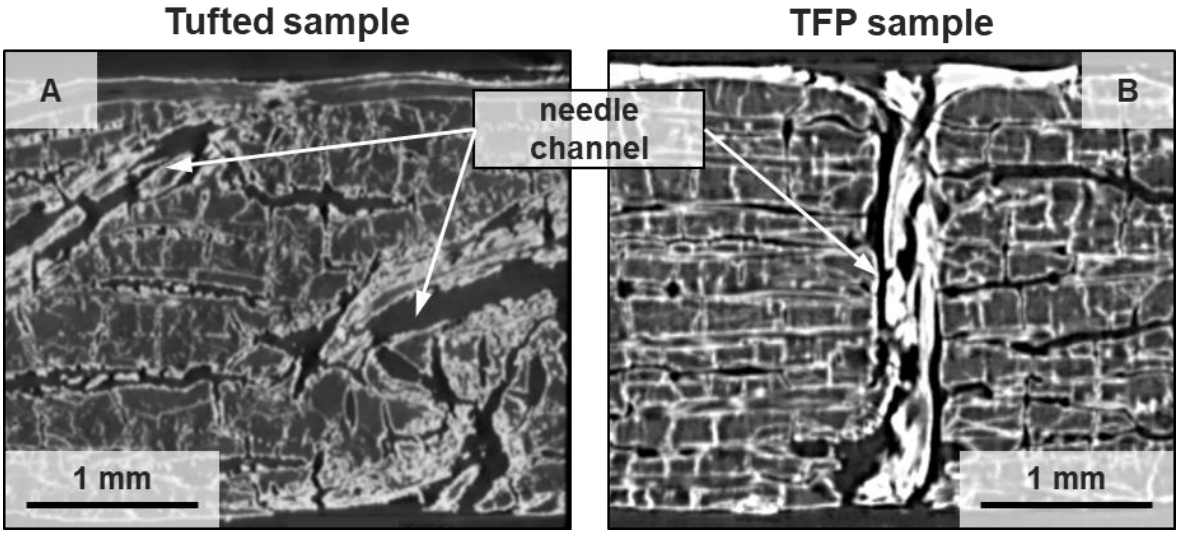

Fig 2. Microstructures of the tufted sample (left) and the TFP sample (right), with displayed needle channel.

Due to the high deformation observed in the tufted sample, the TFP method was selected for all subsequent investigations. Another factor favouring the discontinuation of tufting was also observed during the tufting process itself. Tufting requires the use of significantly thicker needles (3 to 4 mm in diameter) compared to the TFP method (0.6 to 1.5 mm) and employs a puncture style that is notably more aggressive than TFP. Consequently, the carbon ply stack experienced considerably greater stress and presumably incurred more severe damage. Additionally, the use of thicker needles in tufting imposes significant limitations on increasing stitch density and utilizing thin yarns. Following the initial screening, nine samples were fabricated using the TFP method with variation in yarn thickness and stich density. Porosity and density (Archimedes method) as well as strength (3PB) were determined for all samples. Microstructure analysis via µCT was conducted on selected samples. To assess the potential for transition control, supersonic absorption and length-specific flow resistance were determined for the sample P(coarse, 50st). Additionally, specific heat capacity and thermal conductivity were determined for the sample using the LFA method.

3.2. Porosity and density

The porosity and density of the ceramic samples were determined using the Archimedes method after pyrolysis and after the final desiliconization. The results for the open porosity of the samples in the desilicated state are presented in Table 1. For the reference sample without stitching yarn, a low porosity in the single-digit range (7.88 %) was observed. Surprisingly, the measured porosity values for the stitching with the fine yarn were only slightly higher (approximately 2 %), or even nearly identical at the lowest stitch density (25 st/cm²). For the medium yarn, the maximum porosity value is only slightly higher by around 5 % (medium, 36 st/cm²) compared to the reference. Particularly

surprising is that the measured porosity values of the coarse yarn are even lower than those of the medium yarn at the same stitch density. Two factors are presumably responsible for this result. Anticipating the results of microstructure analysis, firstly, the residue of the aramid yarn is responsible. The residue is higher than initially assumed, as indicated in **Fig. 2B** (microstructure of the TFP sample). Consequently, the needle channel, which should account for a significant portion of the porosity, is sealed and not available as porosity. The second effect is that during siliconization and the reaction of carbon and silicon to silicon carbide, particularly small pores are sealed. This reaction-coupled pore sealing leads to a higher variance in porosity within the sample bodies. This effect has already been described by Dittert et al., and they proposed that a clearer examination is possible in the C/C state [10]. Therefore, to obtain a better understanding of the influence of the process parameters stitch density and yarn thickness, the porosity results in the C/C state are provided in Table 2. Since pore sealing through the siliconization process has not yet occurred here, the parameter influence can be better assessed. The porosity value of the reference is around 15 %, and the values for the fine yarn thickness are relatively close to this value (14.2 % - 16.2 %). As in the desiliconized state, porosity increases with increasing stitch density. Thus, the highest porosity value (20.6 %) is measured with the thickest yarn and the highest stitch density (coarse, 50 st/cm²).

Table 1. Open porosity values of the desiliconized C/C-SiC.

stitch density	reference	fine	medium	coarse
0 st/cm²	7.88	-	-	-
16 st/cm²	-	-	-	11.35
25 st/cm²	-	7.82	12.23	11.89
36 st/cm²	-	8.64	12.66	10.99
50 st/cm²	-	10.15	-	12.25

Table 2. Open porosity values of the C/C state during material manufacturing.

stitch density	reference	fine	medium	coarse
0 st/cm²	14.66	-	-	-
16 st/cm²	-	-	-	17.27
25 st/cm²	-	14.16	17.90	18.43
36 st/cm²	-	15.10	19.41	20.07
50 st/cm²	-	16.16	-	20.64

The underlying relationships become clearer when considering porosity across stitch density at constant yarn thickness. This is exemplified in **Fig. 3A**. It can be observed that in the C/C state, there is an increase in porosity with higher stitch density. However, this relationship cannot be definitively determined in the desiliconized state. Plotting porosity against yarn thickness also reveals that porosity increases with higher yarn thickness (**Fig. 3B**). Nevertheless, the results demonstrate that the increase is always minimal and does not occur to the same extent as changes in yarn thickness and stitch density. As previously discussed, the main cause for this is that the puncture areas, despite mass loss during pyrolysis, are still significantly blocked by the residue of the aramid yarn.

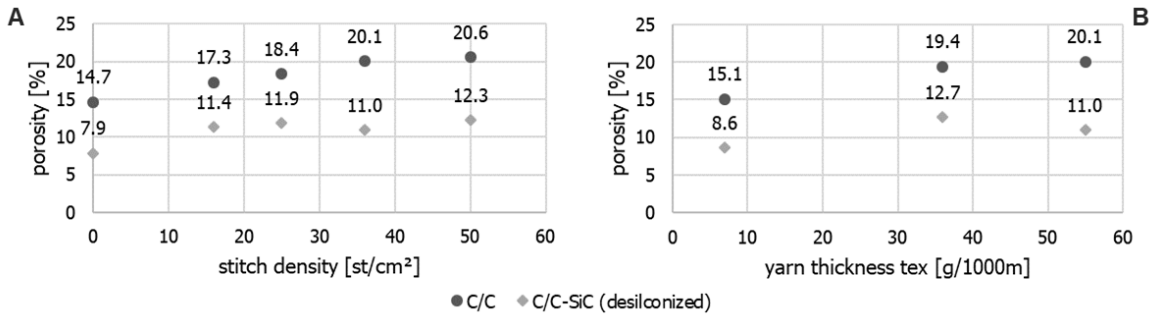

Fig 3. A: Porosity plotted against stich density for coarse yarn (left). B: Porosity plotted against yarn thickness for stich density 50 st/cm² (right).

The density of the material samples was also determined using the Archimedes method and is listed in Table 3 for the desiliconized state. The values range from 1.67 to 1.79 g/cm³, falling within a typical range for desiliconized C/C-SiC. However, no direct dependency of density on the varied process parameters is apparent.

Table 3. Density values of the desiliconized C/C-SiC.

Stitch density	reference	fine	medium	coarse
0 st/cm²	1.75	-	-	-
16 st/cm²	-	-	-	1.69
25 st/cm²	-	1.74	1.67	1.69
36 st/cm²	-	1.73	1.68	1.79
50 st/cm²	-	1.71	-	1.77

3.3. Mechanical characterization

To provide an initial assessment of the structural mechanical properties, the samples were measured using three-point bending according to standard DIN EN 658-3. The averaged maximum bending stresses (failure) are summarized in Table 4. The reference exhibits a maximum value slightly above 130 MPa. This also represents the highest value among all measured samples. It is evident across all samples that a decrease in strength occurs with increasing stitch density. **Fig. 4A** illustrates the strength plotted against stitch density for the coarse yarn, emphasizing this relationship. At stitch densities of 36 and 50, the strength is already reduced by over 30 % compared to the material produced without aramid yarn. Similarly, when plotting strength against yarn thickness at a constant stitch density (**Fig. 4B**), it is also apparent that there is a tendency for strength to decrease with thicker yarns. However, this effect cannot be conclusively confirmed yet, as there is e.g. nearly identical strength across different yarn thicknesses at a stitch density of 25 st/cm².

Table 4. Bending strength measured by means of 3PB for the desiliconized C/C-SiC, results in MPa.

Stitch density	reference	fine	medium	coarse
0 st/cm²	132.15 ± 20.13	-	-	-
16 st/cm²	-	-	-	114.30 ± 2.47
25 st/cm²	-	107.64 ± 7.10	105.58 ± 4.45	107.62 ± 10.30
36 st/cm²	-	104.33 ± 1.36	90.75 ± 18.07	85.44 ± 7.38
50 st/cm²	-	93.60 ± 7.27	-	83.62 ± 12.64

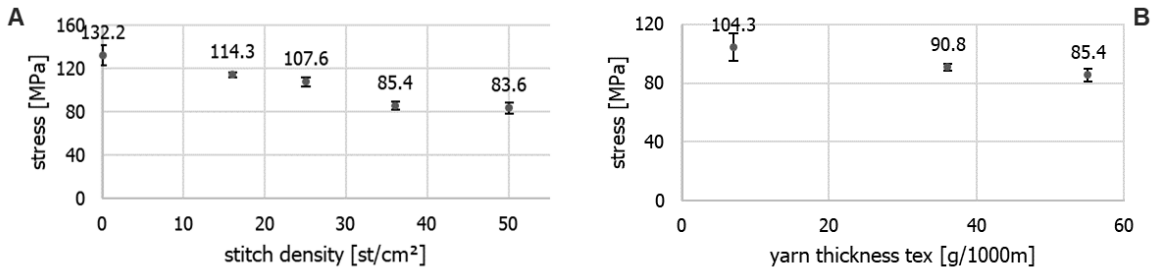

Fig 4. A: Strength plotted against the stitch density for the coarse yarn (left), B: strength plotted against the yarn thickness for the 36 st/cm² samples (right)

Analogous to the fracture strength, the young's modulus was also determined for the tested samples (Table 5). For the reference sample, this value is just under 65 GPa. In all aramid yarn samples, the Young's modulus is lower than this value. While the general trends of decreasing Young's modulus with increasing stitch density or increasing yarn thickness appear to persist similar to the strength, the values are too inconsistent to confidently assert this.

Table 5. Young's modulus for the desiliconized C/C-SiC, results in GPa.

Stitch density	reference	fine	medium	coarse
0 st/cm²	65.69 ± 9.50	-	-	-
16 st/cm²	-	-	-	64.98 ± 2.21
25 st/cm²	-	64.82 ± 2.02	58.18 ± 2.54	59.26 ± 4.56
36 st/cm²	-	64.30 ± 6.35	48.03 ± 4.15	48.30 ± 3.62
50 st/cm²	-	59.43 ± 1.28	-	50.53 ± 4.95

3.4. Microstructure analysis (µ-CT)

Microstructural analysis was conducted using computed tomography on the final material (desiliconized C/C-SiC). Selected samples with coarse yarn were used to analyze the effect of increased stitch density. **Fig. 5** depicts the material cross-sections for the lowest and highest stitch densities. The scans clearly illustrate the penetration areas of the yarn from the stitching process. It is noticeable that despite the clearly visible needle channels, residues of the aramid yarn remain prominently in the material. In these areas, the needle channels are partially closed, significantly affecting continuous porosity, contrary to initial expectations. **Fig. 5A** and **5C** show that the impact of increased stitch density during the stitching process results in more needle channels. Furthermore, it can be observed that horizontal pore channels are present in the in-plane view. However, sections B and D reveal that outside the needle channel

layer, almost no horizontal pores are present. Pores are only visible where needle channels run parallel to the image plane, deeper into the material. Therefore, it is concluded, that porosity occurs only in a cross-shaped orientation relative to the needle channel axis.

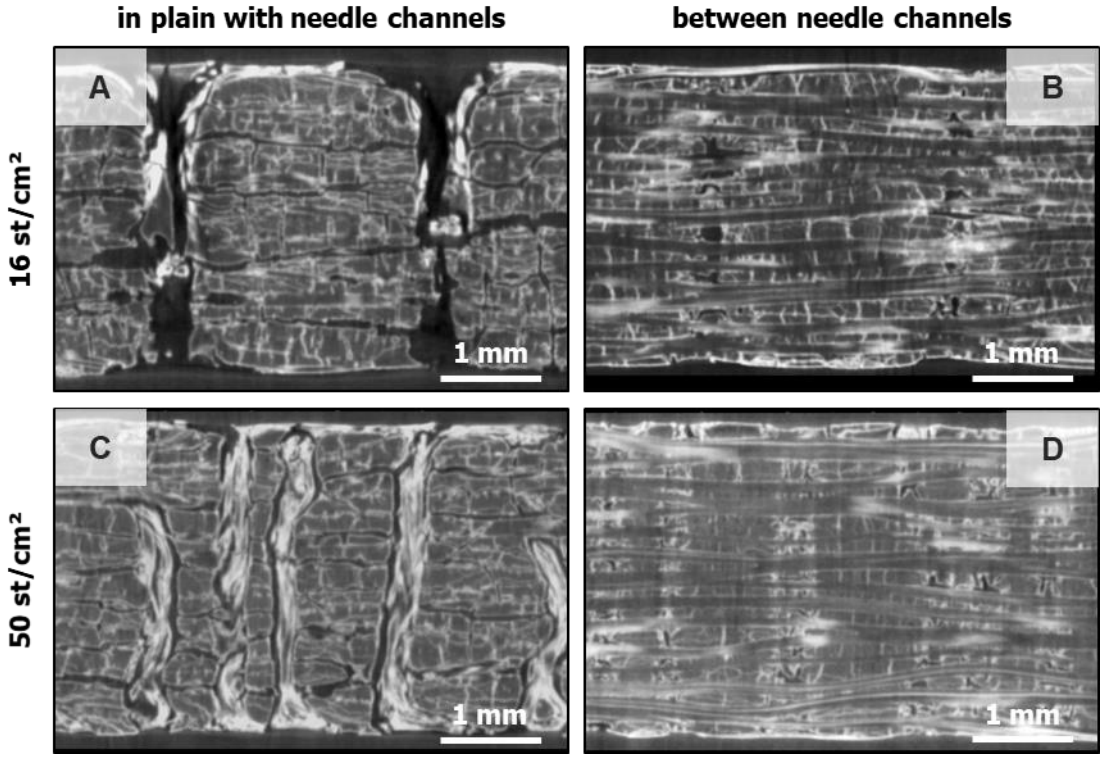

Fig 5. Microstructures of desiliconized C/C-SiC samples with coarse yarn for different stich densities (16 st/cm² and 50 st/cm²) in needle channel plain (A and C) and out of needle plain (B and D) (grey- white = material, black = porosity).

To further visualize this effect, **Fig. 6** shows the top view of the material at 16 st/cm². Here, the cross-shaped pore formation is even more evident. However, it is apparent that the pore formation is not strictly symmetrical but varies significantly across the ply stack.

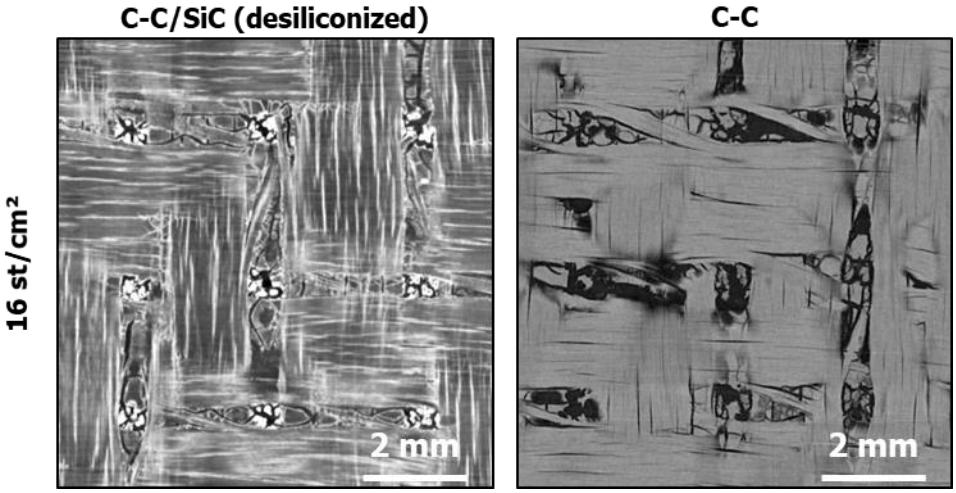

Fig 6. Top view of coarse yarn sample (16 st/cm²) after desiliconization (left) and after pyrolysis (right).

To even better visualize the described effects, the samples were also examined in the C/C state using CT scans (**Fig. 7**). Here, the effects of aramid yarn residue and horizontal pore branching from the

needle channels become even more pronounced. Additionally, in **Fig. 7C**, it can be observed that not all needle stitches reach the bottom of the ply stack. Here, the upper and lower thread interlacing does not occur entirely below the ply stack but within it. While this was not desired for these samples, it presents an interesting option whereby pores may not be consistently executed. Depending on the application, pores could be executed to only a sufficient depth to be effective for acoustic absorption, yet not bridge to the lower side of the material, thus preventing complete flow-through.

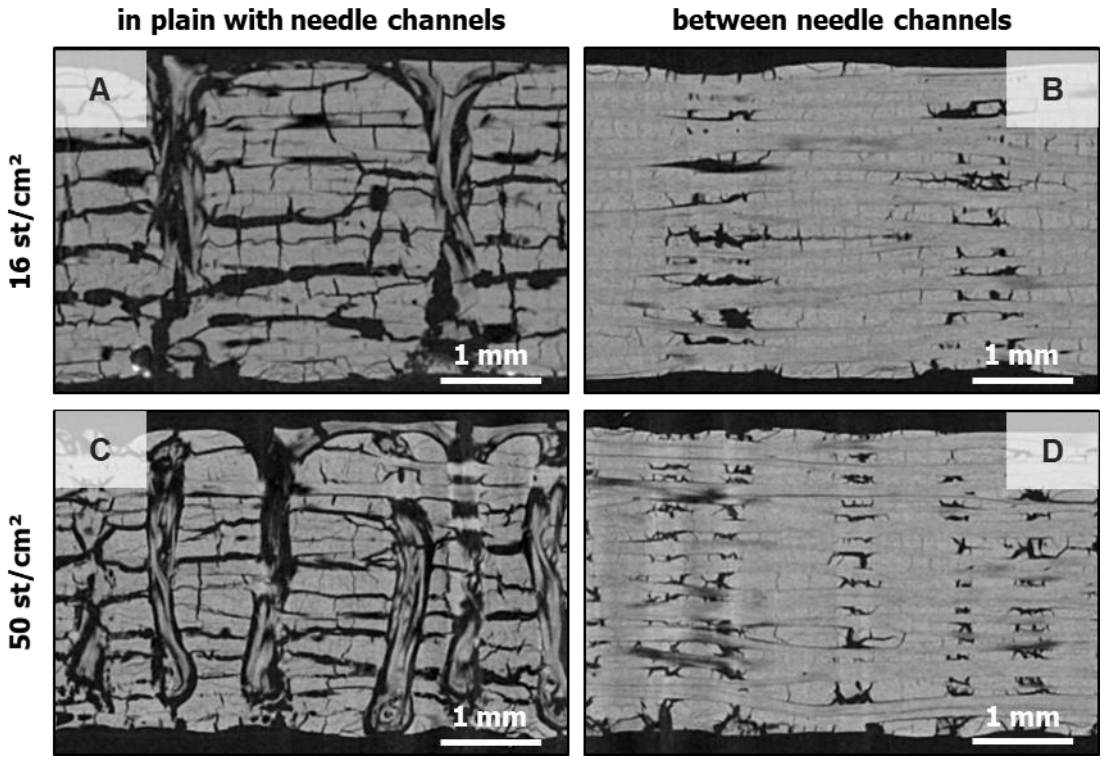

Fig 7. Microstructures of C/C samples with coarse yarn for different stich densities (16 st/cm² and 50 st/cm²) in needle channel plain (A and C) and out of needle plain (B and D) (grey = material, black = porosity).

3.5. Specific thermal capacity and thermal conductivity

The specific heat capacity and thermal conductivity were determined using laser flash analysis (LFA). Due to sample limitations in thickness, values could only be measured in Z direction. In **Fig. 8**, the measurement results for both parameters are depicted. The values of the specific heat capacity are within the typical ranges for regular C/C-SiC materials as described by Shi et al. [2]. However, in the realm of thermal conductivity, the measured values are nearly three times lower than those of regular C/C-SiC. This substantial decrease can be attributed primarily to porosity, which, due to its insulating effect, reduces thermal conductivity. This factor must be considered for future applications, particularly when heat transport throughout the material plays a crucial role in its functionality.

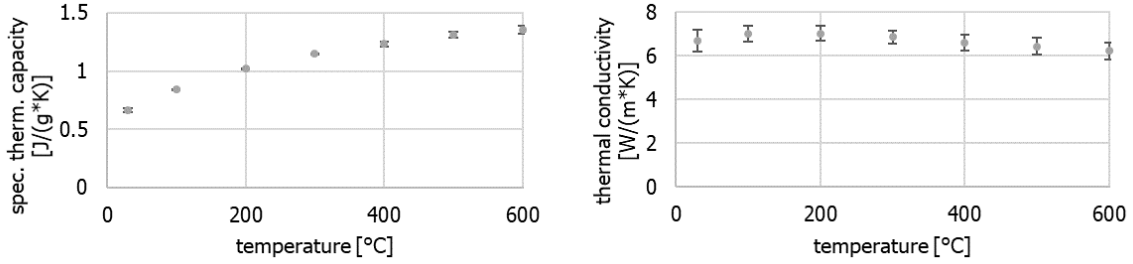

Fig 8. Results of the specific thermal capacity measurement (left), results of the thermal conductivity measurement for the coarse yarn sample with stich density 50 st/cm² (right).

3.6. Supersonic absorption

As a relevant parameter for assessing the transition behaviour, the absorption of the sample P(coarse, 50g/cm²) was determined. The measurements allow for the determination of the acoustic absorption capability as a function of frequency. Results are presented for a static pressure of 15 kPa corresponding to a typical surface pressure of a hypersonic vehicle at sustained flight. The measurement was conducted for frequencies of 125, 300, and 500 kHz. These ranges have been previously identified in literature as relevant for hypersonic applications [4]. The results, presented in **Fig. 9**, reveal a frequency-dependent absorption, where acoustic waves at higher frequencies are better absorbed. Thus, in analogy to prior studies on C/C and C/C-SiC, acoustic absorption was successfully demonstrated for the new material variation [11]. In this context, the new generation of OCTRA appears quite promising in terms of absorption efficiency. However, due to the ongoing challenge of controlling porosity as desired, it remains crucial to continue efforts to eliminate residual aramid in the stitching channels.

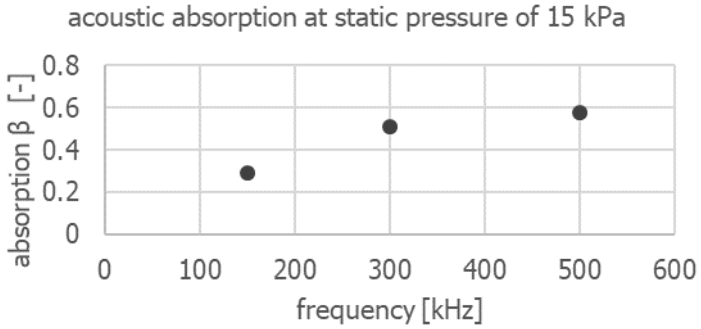

Fig 9. Acoustic absorption at a static pressure of 15 kPa plotted against different frequencies.

3.7. Length specific flow resistance

As another relevant parameter for the absorption properties, the length-specific flow resistance was determined according to DIN EN ISO 9053-1 standards. This parameter is plotted against increasing flow velocity, with the velocity increase caused by the increase in differential pressure. This was determined for sample P(coarse, 50 st/cm²) under normal atmospheric conditions at room temperature (**Fig. 10**). The result of the measurement is a nearly constant length-specific flow resistance of 3.4 MPas/m². In combination with material-specific pore sizes, this also allows for the assessment of material absorption properties. However, since the pore sizes could not be determined, the result only enables a qualitative assessment of material properties. Nevertheless, a lower length-specific flow resistance tends to improve acoustic absorption [10]. Values determined by Dittert et al. for OCTRA produced using the RTM method show flow resistance in the range of 4.94 MPas/m², thus higher. This indicates that with suitable pore geometry and size, the new class of materials has high potential for suitable absorption properties in a relevant frequency range and is therefore of interest for transition control.

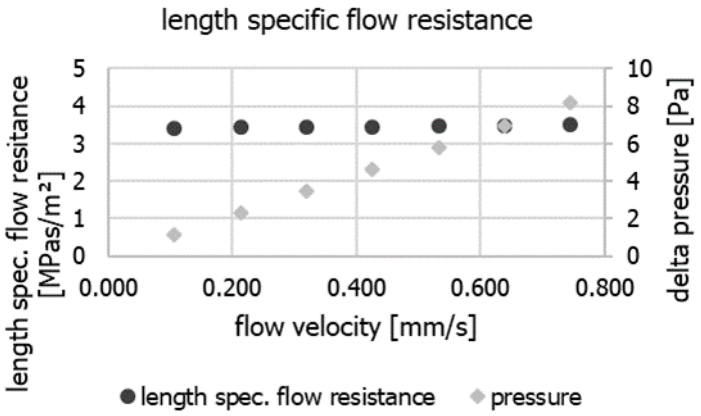

Fig 10. Measurement of the length specific flow resistance plotted against the flow velocity.

4. Conclusion

The results regarding the adjustment of directed porosity in fibre-reinforced ceramics demonstrate promising initial findings. Microstructure examinations, in particular, have showcased the significant potential of the stitching process for porosity control. Among the parameters investigated so far, stitch density has emerged as the most relevant factor. However, it has been demonstrated that the choice of stitching yarn also plays an essential role, as its residue after pyrolysis is crucial in determining whether the needle channels remain open (as pores) or are partially blocked. Further investigations must, therefore, consider the aspect of the yarn material itself in order to identify a variant that remains thermally stable during shaping, thereby preserving the pore network, yet allows for the needle channels to remain largely unobstructed during pyrolysis due to a low residual carbon content. In addition to these findings, initial measurements of the absorption properties and length specific flow resistance have been conducted. The summarized results have provided promising initial findings and suggest that OCTRA adjusted via TFP is an intriguing material worthy of further development. Therefore, this work indicates the direction for further research aimed at achieving significantly more efficient functionalization of C/C-SiC, to target specific needs for hypersonic applications.

Acknowledgments

The presented research was supported by the Research Institute for Materials, Fuels and Lubricants (WIWeB) of the German Bundeswehr and the German Aerospace Center, Institute of Structures and Design

References

[1] R. Kochendörfer, *Liquid Silicon Infiltration- A Fast and Low Cost CMC- Manufacturing Process*. 1991.

[2] Y. Shi, F. Kessel, M. Frieß, N. Jain, and K. Tushtev, "Characterization and modeling of tensile properties of continuous fiber reinforced C/C-SiC composite at high temperatures," *Journal of the European Ceramic Society,* vol. 41, 10/02 2020, doi: 10.1016/j.jeurceramsoc.2020.09.043.

[3] A. Wagner, K. Hannemann, and V. Wartemann, "Hypersonic boundary-layer stabilization by means of ultrasonically absorptive carbon-carbon material Part 1: Experimental Results," in *51st AIAA Aerospace Sciences Meeting including the New Horizons Forum and Aerospace Exposition*.

[4] A. Wagner, K. Hannemann, and M. Kuhn, "Ultrasonic absorption characteristics of porous carbon–carbon ceramics with random microstructure for passive hypersonic boundary layer

transition control," *Experiments in Fluids,* vol. 55, 06/01 2014, doi: 10.1007/s00348-014-1750-4.

[5] V. Wartemann, H. Luedeke, and N. Sandham, "Numerical Investigation of Hypersonic Boundary-Layer Stabilization by Porous Surfaces," *AIAA Journal,* vol. 50, pp. 1281-1290, 06/01 2012, doi: 10.2514/1.J051355.

[6] M. Kuhn *et al.*, *Ceramic Strut Injection Technologies for High-Speed Flight*. 2017.

[7] H. Boehrk, "Transpiration Cooling at Hypersonic Flight - AKTiV on SHEFEX II," in *11th AIAA/ASME Joint Thermophysics and Heat Transfer Conference*.

[8] C. Dittert and M. Kütemeyer, "Octra - Optimized Ceramic for Hypersonic Application with Transpiration Cooling," in *Advances in High Temperature Ceramic Matrix Compo sites and Materials for Sustainable Development; Ceramic Transactions, Volume CCLXIII*, 2017, pp. 389-399.

[9] F. H. Gern and R. Kochendörfer, "Liquid silicon infiltration: description of infiltration dynamics and silicon carbide formation," *Composites Part A: Applied Science and Manufacturing,* vol. 28, no. 4, pp. 355-364, 1997/01/01/ 1997, doi: https://doi.org/10.1016/S1359-835X(96)00135-2.

[10] C. Dittert, M. Kütemeyer, M. Kuhn, and A. Wagner, "Process Optimization of Ceramic Matrix Composites for Ultrasonically Absorptive TPS Material," in *2018 Joint Thermophysics and Heat Transfer Conference*.

[11] A. Wagner, V. Wartemann, M. Kuhn, C. Dittert, and K. Hannemann, "The Potential of Ultrasonically Absorptive TPS Materials for Hypersonic Vehicles," in *20th AIAA International Space Planes and Hypersonic Systems and Technologies Conference*.

